Chemistry–A European Journal | Research Article
doi.org/10.1002/chem.202200576
Chemistry Europe
European Chemical Societies Publishing

www.chemeurj.org

Highly Deep-Blue Luminescent Twisted Diphenylamino Terphenyl Emitters by Bromine-Lithium Exchange Borylation-Suzuki Sequence

Julia Wiefermann,[a] Philipp Schmeinck,[b] Christian Ganter,[b] and Thomas J. J. Müller*[a]

Dedicated to Prof. Dr. Herbert Mayr on the occasion of his 75th birthday

Abstract: Four novel intensively blue luminescent chromophores were readily synthesized by bromine-lithium exchange borylation-Suzuki (BLEBS) sequence in moderate to good yields. Their electronic properties were studied by absorption and emission spectroscopy and quantum chemical calculations revealing deep-blue emission in solution as well as in the solid state and upon embedding into a PMMA (polymethylmethacrylate) matrix with small FWHM (full width at half maximum) values and CIE y values smaller than 0.1. Moreover, high photoluminescence quantum yields (PLQY), partially close to unity, are found.

Introduction

Over the past decades organic electronics are in the focus of scientific and industrial research.[1] Due to flexible processability and the absence of toxic and expensive heavy metals, organic functional chromophores offer important advantages with respect to sustainability and applicability.[2] Various organic molecules already found entry in organic light-emitting diodes (OLEDs),[3] organic field-effect transistors,[4] and organic photovoltaics,[5,6] or in sensor arrays for bio and environmental analytics.[7] Especially, efficient deep-blue emitters for OLEDs are highly demanded due to their indispensability for high-quality displays and lighting sources.[8] Triphenylamine derivatives have attracted huge interest for such applications.[9] They combine high thermal and photochemical stability.[10] Moreover, triphenylamines are also prominently known as strong donor moieties,[11] and they are often employed in organic emitters, such as thermally activated delayed fluorescence dyes, or in organic solar cells.[11a,12] Furthermore, they are used as hole transport materials due to high hole transport mobility and low ionization potentials.[13,14] On the other hand, benzonitriles constitute very well-known acceptor moieties for designing highly luminescent fluorophores.[15] In 2020, Xu et al. reported a deep-blue emitting compound based on triphenylamine, a benzonitrile acceptor and 9,9-dioctylfluorene as a π-conjugation unit.[16] Another class of blue emitters are spiroconjugated chromophores also including triphenylamines as a structure motif.[17,18] Often the synthesis of fluorophores requires multistep synthesis with many purification steps, which is tedious and lacks efficiency. Herein, we present a one-pot synthesis of four highly blue luminescent diphenylamino terphenyl based donor-acceptor conjugates with extended π-systems. In addition, their remarkable photophysical properties as well as the rationalized electronic structure by TD-DFT calculations are presented.

Results and Discussion

Synthesis

One-pot methodologies represent an economical and efficacious way to functional donor-acceptor chromophores.[12a] Based on the structure of the TADF emitter published by our group in 2018, which imposes conformational torsion on the donor-acceptor conjugate[12a] we became interested in comparing effects of extended π-conjugation with concomitant steric hindrance by four novel designed chromophores. The bromine-lithium exchange borylation-Suzuki (BLEBS) sequence[19] promises a practical, concise access to emitters consisting of extended π-systems of benzonitrile acceptor and triphenylamine donor moieties. Here, the BLEBS sequence commences from 4-bromo-3-methyl-*N*,*N*-diphenylaniline (**1**),[20] where the reaction conditions are adapted due to the steric hindrance of the coupling partners.

Upon reaction with potassium *tert*-butoxide as a base the *p*-phenylene bridged compounds **3a** and **3b** are obtained (60

[a] J. Wiefermann, Prof. Dr. T. J. J. Müller
Institut für Organische Chemie und Makromolekulare Chemie, Heinrich-Heine-Universität Düsseldorf
Universitätsstraße 1, D-40225 Düsseldorf (Germany)
E-mail: ThomasJJ.Mueller@hhu.de

[b] P. Schmeinck, Prof. Dr. C. Ganter
Institut für Anorganische Chemie und Strukturchemie I, Heinrich-Heine-Universität Düsseldorf
Universitätsstraße 1, 40225 Düsseldorf (Germany)

Supporting information for this article is available on the WWW under https://doi.org/10.1002/chem.202200576

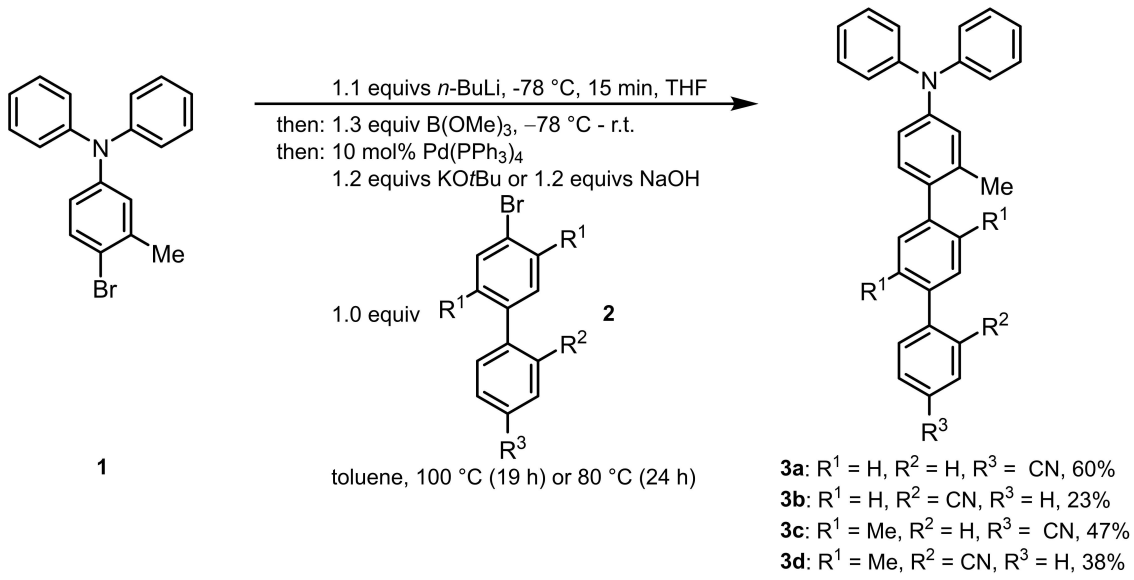

Scheme 1. BLEBS-sequence for the synthesis of *p*-arylene-bridged triarylamino donor-benzonitrile conjugates **3**.

and 23%). Due to thorough purification the yield of compound **3b** is low. Whereas the synthesis of the *p*-xylylene bridged compounds **3c** and **3d** is successfully accomplished (47 and 38%) with sodium hydroxide as a base and toluene as a cosolvent in the Suzuki step. The structure of the title compounds **3** was unambiguously assigned by extensive ^{1}H and ^{13}C NMR spectroscopy and mass spectrometry. The molecular composition was confirmed by combustion analyses (Scheme 1).

In addition, the structure of compound **3a** was corroborated by an X-ray structure analysis.[21] The colorless block-shaped compound crystallizes conformationally twisted in the triclinic space group P-1. The structure reveals that the molecule adapts a twisted conformation, where the benzonitrile moiety is rotated by an angle of 30.15° against the phenylene ring, which, in turn, is rotated by 51.47° against the tolyl part. The benzonitrile and the tolyl ring planes adopt an angle of 81.27°. Furthermore, in the crystal packing, inversion symmetry related pairs of molecules are arranged in an anti-parallel donor-acceptor alignment (Figure 1). However, the corresponding dipole vectors, which extend between the nitrogen of the diphenylamine and the cyano group within a molecule, do not adopt the electrostatically most favourable eclipsed alignment, but are displaced from each other by approximately 4 Å, providing space for the space filling diphenylamine termini. The shortest intermolecular distance between two aromatic carbon atoms is 3.411 Å, slightly more than twice of the Van der Waals radius of carbon, ruling out the possibility of significant π-π-interactions. The intermolecular shift angle α of the molecular planes accounts to approximately 41°.

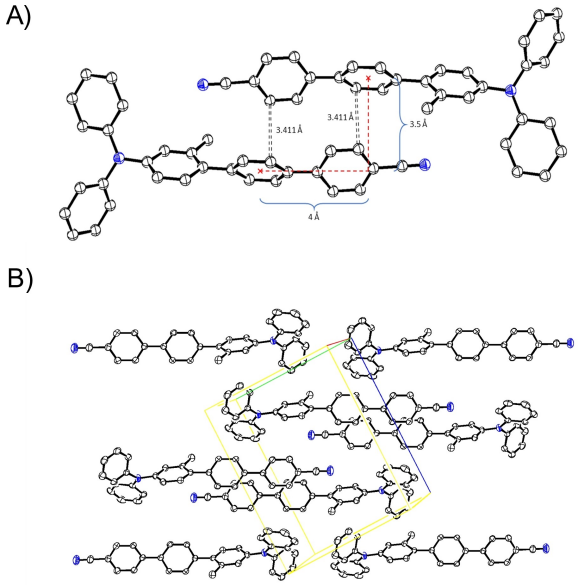

Figure 1. A) X-ray crystal structure of compound **3a** with interplanar distances. Displacement ellipsoids are drawn at the 30% probability level. B) Depiction of crystal packing with unit cell outline of compound **3a** viewed along 100.

Photophysical properties

All four compounds luminesce intensively blue in both solution and the solid state (Figure 2). Therefore, the electronic properties were studied by UV/vis and steady state fluorescence spectroscopy (Figure 3, Table 1).

The absorption spectra in toluene reveal different characteristics for both bridged series **3a**–**b** and **3c**–**d**. While a single absorption maximum around 307 nm appears for compounds

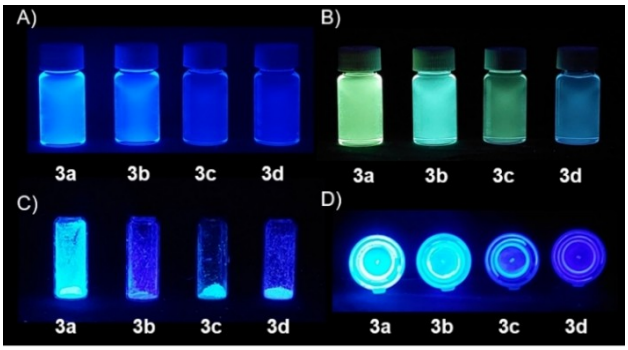

Figure 2. Emission of compounds **3** (λ_{exc} = 365 nm). A) In toluene (c(**3**) = 10^{-4} M). B) In dichloromethane (c(**3**) = 10^{-4} M). C) In the solid state. D) In 1 wt% PMMA films.

3c and **3d** with absorption coefficients ε of 32980 and 35750 M^{-1} cm^{-1}, the spectra of compounds **3a** and **3b** display two bathochromically shifted absorption maxima. The spectrum of compound **3a** shows the two distinctly separated maxima (287 and 339 nm). In the spectrum of compound **3b** besides the maximum at 307 nm a shoulder at 328 nm is detected.

The emission spectra display a dependence of the maxima on the substitution pattern. Characteristically, all compounds exhibit large Stokes shifts ranging from 6300 to 8120 cm^{-1} (Table 1). The emission bands of the *ortho*-cyano substituted compounds **3b** and **3d** are hypsochromically shifted in comparison to the emission bands of the *para*-cyano substituted compounds **3a** and **3c**. Also, the absolute photoluminescence quantum yields reveal distinct differences. The sterically less hindered compounds **3a** and **3b** exhibit high fluorescence quantum yields of 0.99, almost unity. Due to increasing the conformational twist, the fluorescence quantum yields of compounds **3c-d** decrease, where the smallest fluorescence quantum yield (0.44) of compound **3d** is caused by the doubly twisted conformation. The conformational twist causes a diminished coefficient density in the HOMOs of the

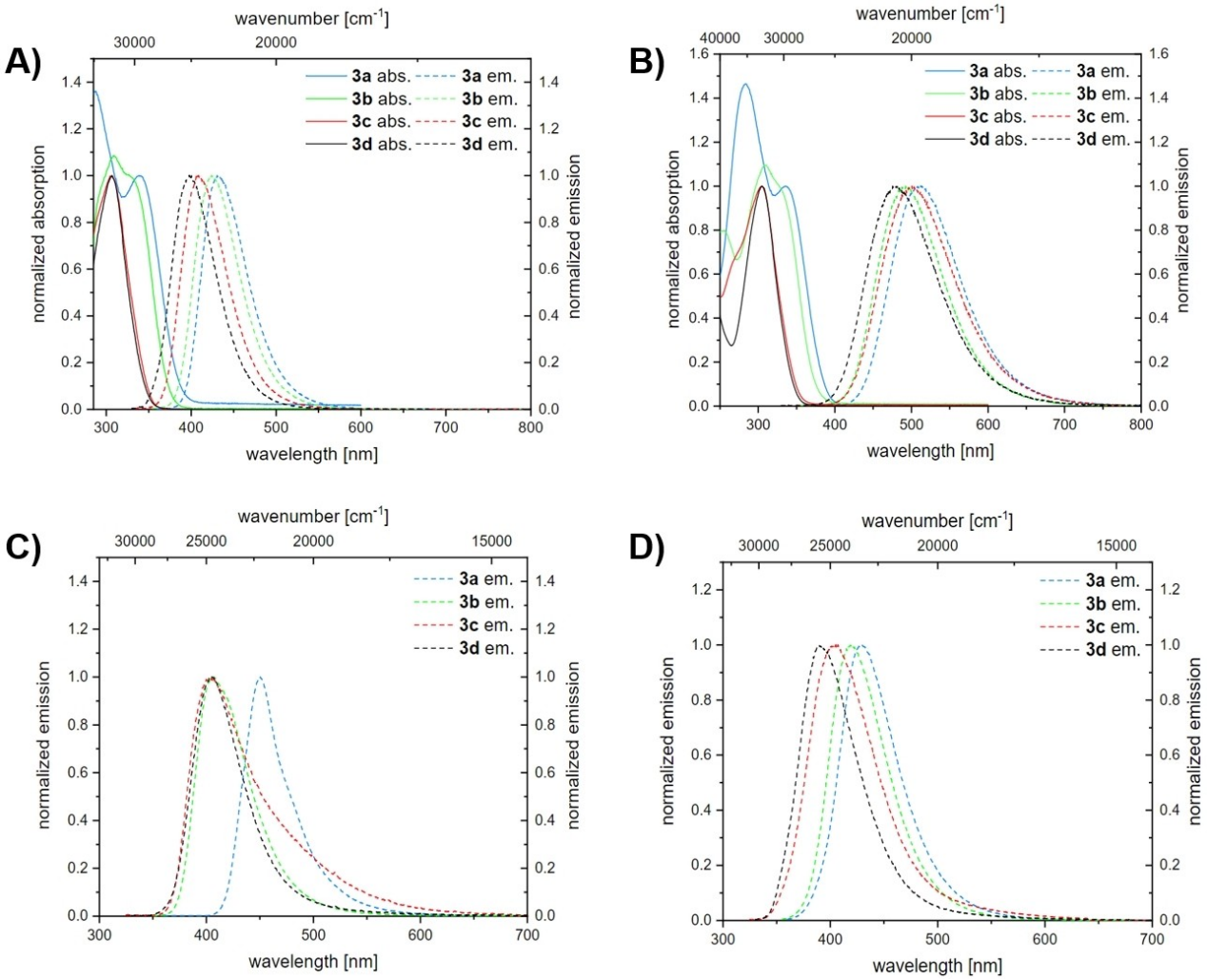

Figure 3. UV/vis absorption (solid lines) and emission spectra (dashed lines) of compounds **3**. A) Recorded in toluene, T = 293 K, c(**3**) = 10^{-5} M for absorption spectra and c(**3**) = 10^{-6} M for emission spectra, $\lambda_{exc} = \lambda_{max,abs}$. B) Recorded in dichloromethane, T = 293 K, c(**3**) = 10^{-5} M for absorption spectra and c(**3**) = 10^{-6} M for emission spectra, $\lambda_{exc} = \lambda_{max,abs}$. C) Emission spectra recorded in the solid state, $\lambda_{exc} = \lambda_{max,abs}$.D) Emission spectra recorded in 1 wt% PMMA films, $\lambda_{exc} = \lambda_{max,abs}$.

Table 1. Selected photophysical properties of compounds **3a–d**.

Entry	$\lambda_{max,abs}$ [nm] (ε [L·mol^{-1}·cm^{-1}])	$\lambda_{max,em}$ [nm] (Φ_{PL})	Stokes shift $\Delta\tilde{\nu}$[a] [cm^{-1}]	FWHM[b] [cm^{-1}] ([eV])	CIE 1931
in toluene [c,d]					
3a	287 (33750), 339 (24830)	431 (0.99)	6300	3159 (0.39)	0.153, 0.059
3b	309 (30250), 328 (27700)	424 (0.99)	6900	3293 (0.41)	0.155, 0.047
3c	307 (35750)	409 (0.83)	8120	3535 (0.44)	0.158, 0.037
3d	307 (32980)	398 (0.44)	7450	3696 (0.46)	0.159, 0.029
in dichloromethane[d,e]					
3a	284 (37360), 336 (25580)	512 (0.99)	10230	3900 (0.48)	0.250, 0.455
3b	309 (30150), 328 (27480)	493 (0.99)	10200	4007 (0.50)	0.195, 0.337
3c	304 (36320)	501 (0.84)	12930	4327 (0.54)	0.226, 0.381
3d	305 (35310)	476 (0.71)	11780	4485 (0.55)	0.186, 0.271
in the solid state[d,f]					
3a	402	450 (0.98)		2271 (0.28)	0.150, 0.088
3b	363	407 (0.77)		3317 (0.41)	0.160, 0.041
3c	357	406 (0.26)		4073 (0.50)	0.169, 0.119
3d	345	405 (0.27)		3262 (0.44)	0.164, 0.012
in 1 wt% PMMA films[d,f]					
3a	362	430 (0.96)		3270 (0.41)	0.155, 0.060
3b	360	420 (0.94)		3394 (0.42)	0.157, 0.048
3c	328	405 (0.38)		4249 (0.53)	0.165, 0.068
3d	320	390 (0.20)		3945 (0.49)	0.165, 0.052

[a] $\Delta\tilde{\nu} = \frac{1}{\lambda max,abs} - \frac{1}{\lambda max,em}$. [b] full width at half maximum [c] Recorded in toluene, $T = 293$ K, $c(\mathbf{3}) = 10^{-5}$–10^{-6} M, $\lambda_{exc} = \lambda_{max,abs}$. [d] Absolute quantum yields determined using an integrating sphere. [e] Recorded in dichloromethane, $T = 293$ K, $c(\mathbf{3}) = 10^{-5}$–10^{-6} M, $\lambda_{exc} = \lambda_{max,abs}$ [f] Recorded at $T = 293$ K, $\lambda_{exc} = \lambda_{max,abs}$.

acceptor parts of **3c–d**, which can be seen in the Kohn-Sham orbitals (see also Supporting Information, Figure S29)

Similarly, as in toluene, dyes **3c–d** display in dichloromethane a single absorption band at 304 nm with molar extinction coefficients ε of 36320 and 35310 M^{-1} cm^{-1} and the sterically less hindered compounds **3a–b** possess an additional maximum at higher energy. The two absorption maxima are well separated for compound **3a**, whereas in the case of compound **3b** a shoulder is detected. The maxima at higher energy also differ in their intensity. The *para*-cyano substitution in the acceptor part leads to a significant increase in intensity and the absorption coefficients ε span from 25580 to 37360 M^{-1} cm^{-1} for the higher energy band of compound **3a**. The emission maxima in dichloromethane appear in a shorter range than in toluene. The emission bands of *ortho*-cyano substituted compounds are hypsochromically shifted compared to the emission band of the *para*-cyano substituted dyes. Fluorescence quantum yields increase for compound **3d** compared to toluene solutions, whereas compounds **3a–b** remain almost the same. Moreover, enormous *Stokes* shifts between 10200 and 12930 cm^{-1} can be determined (Table 1).

While the emission maxima of dyes **3b**, **3c**, and **3d** in the solid state lie closely between 405 and 407 nm compound **3a** fluoresces with a strongly bathochromically shifted maximum at 450 nm. In addition, the emission spectra of compounds **3a** and **3c** reveal a shoulder at longer wavelength, which is more pronounced for compound **3c**. This can also be underlined by the higher value of FWHM (full width at half maximum) of 4073 cm^{-1}. The smallest FWHM with 2271 cm^{-1} is assigned to the emission band of compound **3a**. It fluoresces with a clear blue color. In general, the emission band widths are smaller for the sterically less hindered compounds **3a–b**. However, a similar trend in FWHM cannot be detected. Absolute fluorescence quantum yields of dyes **3c–d** are moderate (0.26) and amount to 0.98 for compound **3a** (Table 1). The small FWHM and the outstanding fluorescence quantum yield qualifies this compound for further investigation in a device as new OLED emitter.

Moreover, all compounds show blue emission with narrow emission bands with a FWHM of 3159–3696 cm^{-1}, exhibiting clear colors in the region of dark blue and the most saturated emission thereby is observed for compound **3d** (Figure 4A). In addition, all compounds fulfill the requirement of a CIE y-coordinate of smaller than 0.1.[8a] Favorably, the smaller the y-value the lower the power consumption of a device.[8b] The CIE coordinates are also close to the standard blue point (0.15, 0.06) for electroluminescence (EL) recommended by the European Broadcast Union (EBU).[22]

The strongly bathochromically shifted emission in dichloromethane to sky-blue or greenish emission (Figure 2B) indicates a positive emission solvatochromicity.[23] The excited state is better stabilized in more polar solvents, such as dichloromethane in comparison to toluene, causing a redshifted emission in dichloromethane. For elucidating the charge transfer character of the chromophores, the absorption and emission behavior was studied in dichloromethane (Figure 3B). The FWHM increases up to 4485 cm^{-1}. These broader emission bands and the strong bathochromic shift underline the charge transfer character of the excited state. The CIE diagram shows the range of emission colors from blue to green for all compounds (Figure 4B). Generally, the emission of *para*-cyano substituted fluorophores is shifted to the green, whereas the emission of the *ortho*-cyano substituted fluorophores remains blue or sky-blue.

According to the CIE diagram for all compounds **3** deep-blue emission in the solid state is shown (Figure 4C). Especially compounds **3a** and **3b** are promising substances due to their high fluorescence quantum yields and small FWHM values. As

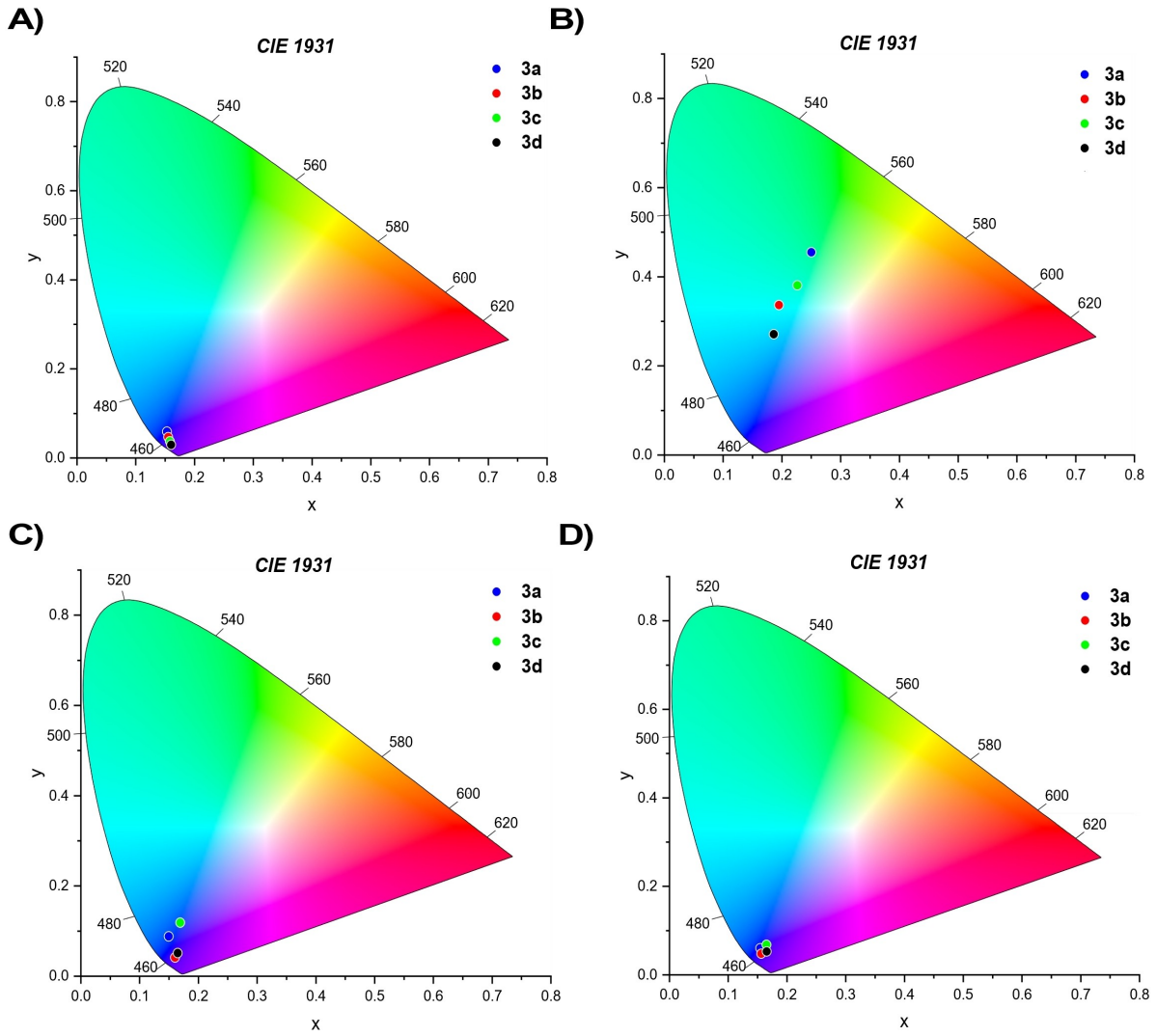

Figure 4. CIE diagrams of the emission of compounds **3**. A) In toluene. B) In dichloromethane. C) In the solid state. D) In 1 wt% PMMA films.

seen in the CIE diagram the emission colors are deep-blue, and especially the emission color of compound **3b** is close to saturated blue. Generally, the emission bands for *para*-cyano substituted fluorophores **3a** and **3c** are bathochromically shifted.

As potential OLED emitters all compounds were embedded in a PMMA matrix with an average molecular weight of 120000 Da. All films luminesce with blue colors (Figure 2D). The emission is significantly affected by the matrix. The general trend for the prediction of emission behavior is confirmed. Compounds **3b** and **3d** emit at higher energy compared to their *para*-cyano substituted analogues and the line shapes of the emission spectra are quite similar (Figure 3D).

The emission of compound **3c** appears around the same energy (405 nm) as in the solid state (406 nm) with a similar FWHM value of 4249 cm^{-1}. Embedding in a rigid PMMA matrix suppresses non-radiative processes.[24] For compound **3c** this results in a higher quantum yield of 0.38 compared to the solid state emission (0.26). On the other hand, the emission of compound **3d** in PMMA is significantly blueshifted to 390 nm in comparison to the solid state (405 nm) and FWHM increases from 3262 to 3945 cm^{-1} in the matrix. Similar observations with increasing FWHM are found for compounds **3a**–**b**. Especially, their quantum yields are remarkably high and with values of 0.96 and 0.94, resp., close to unity. A significant increase in PLQY in comparison to the solid state is detected for compound **3b**. The CIE diagram clarifies the clear blue emission colors for all compounds with a nearly saturated color for each compound, however, compound **3b** shows the most saturated emission color in the series (Figure 4D). Nevertheless, compound **3a** is remarkably close to the standard blue point set by the EBU.[22] Due to these results for a more polar matrix, for example PVC (polyvinyl chloride), higher y-values of the compounds would be expected, whereas for a more unpolar matrix like PS (polystyrene) higher x-values are probably evoked by the matrix.

The luminescence properties were further investigated by lifetime measurements (Figure 5). All decays could be fitted by

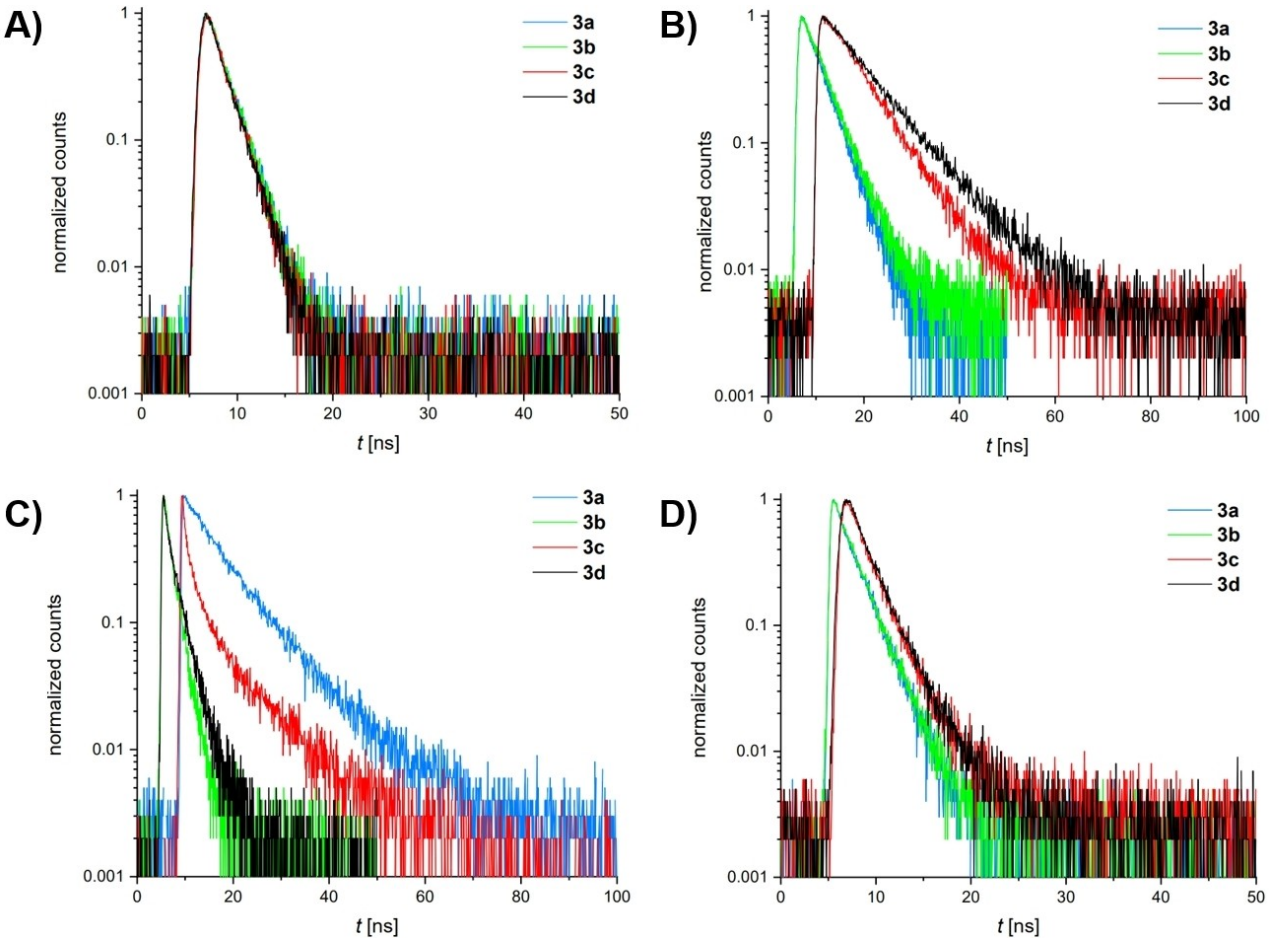

Figure 5. Lifetime measurements of compounds **3a-d**. A) In toluene. B) In dichloromethane. C) In the solid state. D) In 1 wt% PMMA films.

a monoexponentially curve. As can be seen the fluorescence lifetimes in toluene are nearly the same range of 1.61–1.86 ns (Figure 5A). For compounds **3a** and **3b** the radiative rate constant (k_r) is two powers of ten higher than the non-radiative rate constant (k_{nr}) (Table 2).[25] This is attributable to the lesser twisting of these compounds. In case of compound **3d** rate constant k_{nr} (3.15×10^8 s^{-1}) is slightly higher than k_r with 2.47×10^8 s^{-1}. The transitions are competitive in the same order.

With increasing solvent polarity, the lifetimes increase for each compound (Figure 5B). Especially for compounds **3c** and **3d** the lifetimes strongly increase up to 6.93 ns and 9.39 ns. Rate constant k_r of compound **3c** is four times smaller than in toluene. Rate constants k_r and k_{nr} for compound **3d** decrease, but in dichloromethane k_r is two times larger (7.56×10^7 s^{-1}) than k_{nr} (3.09×10^7 s^{-1}). Rate constants k_r and k_{nr} for compounds **3a** and **3b** are halved, but the ratio remains constant (Table 2).

Moreover, solid state emission occurs with long fluorescence lifetimes, especially for the *para*-substituted compounds **3a** (8.16 ns) and **3c** (9.44 ns) (Figure 5C). For compound **3a** rate constant k_r (1.20×10^8 s^{-1}) is much larger than k_{nr} (2.45×10^6 s^{-1}), which plausibly explains the high quantum yield. Compared to the rate constants of this compound in solution, k_r is decreased (Table 2). The low quantum yields of **3c** and **3d** in

Table 2. Fluorescence lifetimes τ_F and determined radiative (k_r) and nonradiative (k_{nr}) rate constants of compounds **3a–d**.

Entry	τ_F [ns]	k_r [s^{-1}]	k_{nr} [s^{-1}]
in toluene[a]			
3a	1.86	5.32×10^8	5.38×10^6
3b	1.66	5.96×10^8	6.02×10^6
3c	1.61	5.16×10^8	1.06×10^8
3d	1.78	2.47×10^8	3.15×10^8
in dichloromethane[b]			
3a	3.91	2.53×10^8	2.56×10^6
3b	4.22	2.35×10^8	2.37×10^6
3c	6.93	1.21×10^8	2.31×10^7
3d	9.39	7.56×10^7	3.09×10^7
in the solid state[c]			
3a	8.16	1.20×10^8	2.45×10^6
3b	1.69	4.56×10^8	1.36×10^8
3c	9.44	2.75×10^7	7.84×10^7
3d	2.29	1.18×10^8	3.19×10^8
in 1 wt% PMMA films[c]			
3a	2.22	4.32×10^8	1.80×10^7
3b	2.05	4.59×10^8	2.93×10^7
3c	2.34	1.62×10^8	2.65×10^8
3d	2.40	8.33×10^7	3.33×10^8

[a] Recorded in toluene, $T=293$ K, $c(\mathbf{3})=10^{-6}$ M [b] Recorded in dichloromethane, $T=293$ K, $c(\mathbf{3})=10^{-6}$ M [c] Recorded at $T=293$ K.

the solid state correlate with high values of rate constant k_{nr}. For compound **3c** rate constant k_{nr} (7.84×10^7 s^{-1}) is approximately three times higher than k_r (2.75×10^7 s^{-1}). Embedding in the PMMA matrix equalizes fluorescence lifetimes to approximately 2 ns for each compound (Figure 5D). For compound **3b** rate constant k_r does not change, but k_{nr} decreases, which results in a higher quantum yield. The difference between rate constants k_r and k_{nr} decreases and additionally the rate constants get larger in case of compound **3c** (Table 2). The results look different in the case of compound **3d**. The radiative rate constant k_r slightly decreases to 8.33×10^7 s^{-1} whereas k_{nr} increases to 3.33×10^8 s^{-1} resulting in a smaller quantum yield than in the solid state.

Calculated Electronic Structure

For scrutinizing the electronic structures of the luminophores, first quantum chemical calculations with the structures **3** were performed with Gaussian 09 to identify the minimum energy conformation.[26] The calculated ground state conformation of compound **3a** is in good agreement with the dihedral angle determined by the x-ray structure analysis. TD-DFT calculations were carried out on DFT-optimized ground state structures. A screening of functionals of the best fit with the experimental data suggests that functional cam-B3LYP[27] and Pople's 6–311++G** basis set[28] can be employed. The absorption maxima in toluene and dichloromethane are very well reproduced using the implicit polarized continuum model (PCM) for inclusion of solvents effects (Table 3).[29] According to TD-DFT calculations the longest wavelength absorption bands are characterized as HOMO to LUMO+X transitions, indicating a locally excited singlet (^{1}LE) state of the triphenylamine donor. Only for compounds **3a** and **3b** HOMO-LUMO transitions are involved in toluene as well as in dichloromethane. These absorption bands reveal a singlet charge transfer (^{1}CT) character and their Kohn-Sham frontier molecular orbitals can be visualized (see Supporting Information, Figure S29). Furthermore, the HOMO and LUMO energy levels in toluene and dichloromethane are very similar.

In addition, the frontier molecular orbitals and the percentage orbital contribution indicate that the compounds are hybridized local and charge transfer (HLCT) excited states materials (see Supporting Information, Figure S30, S31). However, these aspects will remain the topic of in depth quantum chemical calculations.

The trend to higher HOMO and LUMO energy levels for the *ortho*-cyano substituted compounds is observed in toluene and dichloromethane. The redshift of the absorption bands of compounds **3a** and **3b** correlates well with the smaller energy difference (ΔE) of the involved orbitals, whereas the blueshift of the absorption maxima of compounds **3c** and **3d** results from non-significant participation of the HOMO-LUMO transition.

The difference plot clarifies the coefficient density change in toluene from the ground to the first excited state (S_1) (Figure 6). It becomes clear that the HOMO-LUMO contribution to the $S_0\rightarrow S_1$ transition of compounds **3a** and **3b** reveal a strong charge transfer character. For compounds **3c** and **3d** the ^{1}LE state of the triphenylamine represents the most dominant contribution to the longest wavelength absorption band and which is not affected by solvent polarity.

The overlap of frontier molecular orbitals is affected by the fluorophore's conformation. Due to steric hindrance the torsion angles between the donor and acceptor moiety are significantly increased for compounds **3c** and **3d**.

Table 3. Selected experimental absorption bands and TD-DFT calculated absorption maxima of the compounds **3** in toluene and dichloromethane (cam-B3LYP, 6-311++G**).

Entry	$\lambda_{max,abs}$ [nm] (ε [L·mol^{-1}·cm^{-1}])	$\lambda_{max,calcd}$ [nm] (oscillator strength)	Most dominant contributions
in toluene			
3a	339 (24830)	306 (1.0857)	HOMO→LUMO (37%)
			HOMO→LUMO+3 (42%)
	287 (33750)	297 (0.0418)	HOMO→LUMO+1 (55%)
3b	328 (27700)	301 (0.8117)	HOMO→LUMO (21%)
			HOMO→LUMO+1 (24%)
			HOMO→LUMO+4 (29%)
	309 (30250)	297 (0.0779)	HOMO→LUMO+2 (64%)
			HOMO→LUMO+6 (12%)
3c	307 (35750)	296 (0.0358)	HOMO→LUMO+2 (66%)
3d	307 (32980)	296 (0.0344)	HOMO→LUMO+2 (68%)
in dichloromethane			
3a	336 (25580)	305 (1.1016)	HOMO→LUMO (38%)
			HOMO→LUMO+2 (40%)
	284 (37360)	296 (0.0399)	HOMO→LUMO+2 (65%)
			HOMO→LUMO+4 (6%)
3b	328 (27480)	300 (0.8040)	HOMO→LUMO (21%)
			HOMO→LUMO+1 (28%)
			HOMO→LUMO+3 (13%)
	309 (30150)	296 (0.0752)	HOMO→LUMO+2 (70%)
			HOMO→LUMO+4 (5%)
3c	305 (35310)	298 (0.0335)	HOMO→LUMO+1 (77%)
3d	304 (36320)	296 (0.0328)	HOMO→LUMO+1 (77%)

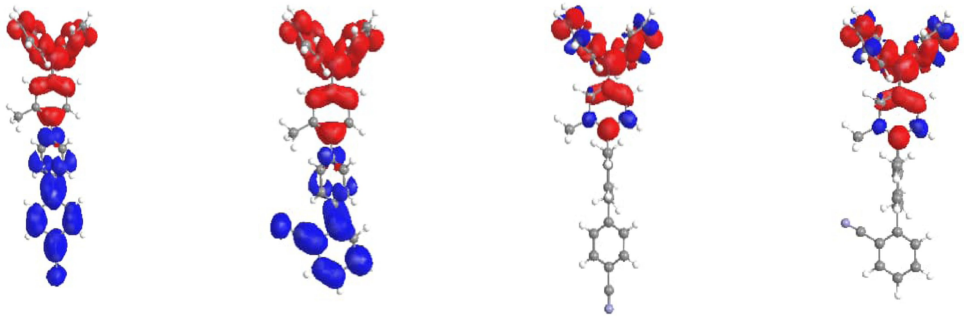

Figure 6. Difference plots for the ^{1}CT and ^{1}LE states of the longest wavelength absorption band of compounds **3** (in toluene). (isovalue = |0.001|) a loss of coefficient density is indicated red and a gain blue.

Conclusion

The BLEBS sequence offers a concise modular access to novel twisted diphenylamino terphenyl emitters. Their electronic properties (UV/vis and emission spectra) can be plausibly assigned and rationalized by TD-DFT calculations. While the emission of all compounds is highly solvatochromic with large Stokes shifts, the absorption is not affected by solvent polarity. In addition, the chromophores display deep-blue emission with small FWHM values in solution, in the solid state, and embedded in a PMMA matrix with very high quantum yields, close to unity for selected examples. The CIE coordinates lie close to the standard blue point recommended by the EBU and with y-values below 0.1 in a nonpolar environment. Application of these chromophores in OLED devices and the investigation of the nature of the underlying emission processes are currently underway.

Experimental Section

All experimental details, such as referenced and described preparations of starting materials, typical procedures for the syntheses of compounds **3**, and all ^{1}H and ^{13}C NMR spectra, absorption and emission spectra, as well as crystal structure information and quantum chemical calculations are included in the Supporting Information.

Acknowledgements

The authors cordially thank the DFG (RTG 2482, Mu 1088/9-1) and the Fonds der Chemischen Industrie for financial support. Computational support and infrastructure were provided by the "Centre for Information and Media Technology" (ZIM) at the University of Düsseldorf (Germany). Thanks to the CeMSA@HHU (**Ce**nter for **M**olecular and **S**tructural **A**nalytics @ **H**einrich **H**eine **U**niversity) for recording the mass-spectrometric and the NMR-spectroscopic data. Open Access funding enabled and organized by Projekt DEAL.

Conflict of Interest

The authors declare no conflict of interest.

Data Availability Statement

The data that support the findings of this study are available in the supplementary material of this article.

Keywords: cross-coupling · DFT calculations · donor-acceptor systems · fluorescence · terphenyls

[1] S. R. Forrest, *Nature* **2004**, *428*, 911–918.
[2] a) H. Ling, S. Liu, Z. Zheng, F. Yan, *Small Methods* **2018**, *2*, 1800070; b) M. Berggren, D. Nilsson, N. D. Robinson, *Nat. Mater.* **2007**, 6, 3–5; c) S. E. Root, S. Savagatrup, A. D. Printz, D. Rodriquez, D. J. Lipomi, *Chem. Rev.* **2017**, 117, 6467–6499.
[3] a) D. Joly, D. Tondelier, V. Deborde, W. Delaunay, A. Thomas, K. Bhanuprakash, B. Geffroy, M. Hissler, R. Réau, *Adv. Funct. Mater.* **2012**, *22*, 567–576; b) J.-H. Lee, C.-H. Chen, P.-H. Lee, H.-Y. Lin, M. Leung, T.-L. Chiu, C.-F. Lin, *J. Mater. Chem. C* **2019**, *7*, 5874–5888.
[4] a) P. Devibala, R. Dheepika, P. Vadivelu, S. Nagarajan, *ChemistrySelect* **2019**, *4*, 2339–2346; b) C. Xu, J. Zhang, W. Xu, H. Tian, *Mater. Chem. Front.* **2021**, *5*, 1060–1075; c) C. Zong, X. Zhu, Z. Xu, L. Zhang, J. Xu, J. Guo, Q. Xiang, Z. Zeng, W. Hu, J. Wu, R. Li, Z. Sun, *Angew. Chem.* **2021**, *133*, 16366–16372; *Angew. Chem. Int. Ed.* **2021**, *60*, 16230–16236.
[5] a) M. S. Abusaif, M. Fathy, M. A. Abu-Saied, A. A. Elhenawy, A. B. Kashyout, M. R. Selim, Y. A. Ammar, *J. Mol. Struct.* **2021**, *1225*, 129297; b) J. Wang, Z. Zheng, Y. Zu, Y. Wang, X. Liu, S. Zhang, M. Zhang, J. Hou, *Adv. Mater.* **2021**, *33*, e2102787.
[6] L. Zhang, X. Yang, W. Wang, G. G. Gurzadyan, J. Li, X. Li, J. An, Z. Yu, H. Wang, B. Cai, A. Hagfeldt, L. Sun, *ACS Energy Lett.* **2019**, *4*, 943–951.
[7] a) Z. Zhu, D. Tian, P. Gao, K. Wang, Y. Li, X. Shu, J. Zhu, Q. Zhao, *J. Am. Chem. Soc.* **2018**, *140*, 17484–17491; b) W. Xu, M. M. S. Lee, Z. Zhang, H. H. Y. Sung, I. D. Williams, R. T. K. Kwok, J. W. Y. Lam, D. Wang, B. Z. Tang, *Chem. Sci.* **2019**, *10*, 3494–3501.
[8] a) X. Yang, X. Xu, G. Zhou, *J. Mater. Chem. C* **2015**, *3*, 913–944; b) Z. Q. Gao, Z. H. Li, P. F. Xia, M. S. Wong, K. W. Cheah, C. H. Chen, *Adv. Funct. Mater.* **2007**, *17*, 3194–3199; c) Y. Im, S. Y. Byun, J. H. Kim, D. R. Lee, C. S. Oh, K. S. Yook, J. Y. Lee, *Adv. Funct. Mater.* **2017**, *27*, 1603007.
[9] a) J. Zhang, Y. Zhao, H. Xu, Di Zhang, Y. Miao, R. Shinar, J. Shinar, H. Wang, B. Xu, Y. Wu, *J. Mater. Chem. C* **2019**, *7*, 10810–10817; b) X. Zhu, Y. Li, Z. Wu, C. Lin, D. Ma, Z. Zhao, B. Z. Tang, *J. Mater. Chem. C* **2021**, *9*, 5198–5205.
[10] S. Thayumanavan, S. Barlow, S. R. Marder, *Chem. Mater.* **1997**, *9*, 3231–3235.

[11] a) T.-T. Bui, F. Goubard, M. Ibrahim-Ouali, D. Gigmes, F. Dumur, *Beilstein J. Org. Chem.* **2018**, *14*, 282–308; b) F. Dumur, F. Goubard, *New J. Chem.* **2014**, *38*, 2204–2224.
[12] a) G. A. Sommer, L. N. Mataranga-Popa, R. Czerwieniec, T. Hofbeck, H. H. H. Homeier, T. J. J. Müller, H. Yersin, *J. Phys. Chem. Lett.* **2018**, *9*, 3692–3697; b) S. Revoju, S. Biswas, B. Eliasson, G. D. Sharma, *Phys. Chem. Chem. Phys.* **2018**, *20*, 6390–6400.
[13] P. Cias, C. Slugovc, G. Gescheidt, *J. Phys. Chem. A* **2011**, *115*, 14519–14525.
[14] Y. Shirota, H. Kageyama, *Chem. Rev.* **2007**, *107*, 953–1010.
[15] F. Baraket, B. Pedras, É. Torres, M. J. Brites, M. Dammak, M. N. Berberan-Santos, *Dyes Pigm.* **2020**, *175*, 108114.
[16] X. Liu, W. Liu, W. Dongyu, X. Wei, L. Wang, H. Wang, Y. Miao, H. Xu, J. Yu, B. Xu, *J. Mater. Chem. C* **2020**, *8*, 14117–14124.
[17] D. Thirion, M. Romain, J. Rault-Berthelot, C. Poriel, *Mater. Adv.* **2021**, *2*, 1271–1283.
[18] J.-D. Peltier, B. Heinrich, B. Donnio, O. A. Ibraikulov, T. Heiser, N. Leclerc, J. Rault-Berthelot, C. Poriel, *Mater. Chem. Front.* **2022**, *6*, 225–236.
[19] A. Franz, T. Müller, *Synthesis* **2008**, 1121–1125.
[20] X.-L. Li, W. Wu, X.-H. Fan, L.-M. Yang, *RSC Adv.* **2013**, *3*, 12091.
[21] Deposition Number CCDC 2125280 contains the supplementary crystallographic data for this paper. These data are provided free of charge by the joint Cambridge Crystallographic Data Centre and Fachinformationszentrum Karlsruhe Access Structures service.
[22] D. Yu, F. Zhao, Z. Zhang, C. Han, H. Xu, J. Li, D. Ma, P. Yan, *Chem. Commun.* **2012**, 48, 6157–6159.
[23] M. J. Kamlet, J. L. Abboud, R. W. Taft, *J. Am. Chem. Soc.* **1977**, *99*, 6027–6038.
[24] S. Reineke, M. A. Baldo, *Sci. Rep.* **2014**, *4*, 3797.
[25] The Strickler-Berg analysis was performed according to J. R. Lakowicz, *Principles of Fluorescence Spectroscopy*, 3rd ed., Springer, Heidelberg, 2006, pp. 9.
[26] M. J. Frisch, G. W. Trucks, H. B. Schlegel, G. E. Scuseria, M. A. Robb, J. R. Cheeseman, G. Scalmani, V. Barone, B. Mennucci, G. A. Petersson, H. Nakatsuji, M. Caricato, X. Li, H. P. Hratchian, A. F. Izmaylov, J. Bloino, G. Zheng, J. L. Sonnenberg, M. Hada, M. Ehara, K. Toyota, R. Fukuda, J. Hasegawa, M. Ishida, T. Nakajima, Y. Honda, O. Kitao, H. Nakai, T. Vreven, J. A. Montgomery Jr, J. E. Peralta, F. Ogliaro, M. Bearpark, J. J. Heyd, E. Brothers, K. N. Kudin, V. N. Staroverov, R. Kobayashi, J. Normand, K. Raghavachari, A. Rendell, J. C. Burant, S. S. Iyengar, J. Tomasi, M. Cossi, N. Rega, J. M. Millam, M. Klene, J. E. Knox, J. B. Cross, V. Bakken, C. Adamo, J. Jaramillo, R. Gomperts, R. E. Stratmann, O. Yazyev, A. J. Austin, R. Cammi, C. Pomelli, J. W. Ochterski, R. L. Martin, K. Morokuma, V. G. Zakrzewski, G. A. Voth, P. Salvador, J. J. Dannenberg, S. Dapprich, A. D. Daniels, O. Farkas, J. B. Foresman, J. V. Ortiz, J. Cioslowski, D. J. Fox, Gaussian 09, Revision A.02, Gaussian 2009.
[27] T. Yanai, D. P. Tew, N. C. Handy, *Chem. Phys. Lett.* **2004**, *393*, 51–57.
[28] R. Krishnan, J. S. Binkley, R. Seeger, J. A. Pople, *J. Chem. Phys.* **1980**, *72*, 650–654.
[29] G. Scalmani, M. J. Frisch, *J. Chem. Phys.* **2010**, *132*, 114110.

Manuscript received: February 22, 2022
Accepted manuscript online: March 17, 2022
Version of record online: April 7, 2022